Zachary Kober
SULI Fall 2020
Research Paper

Study of x-ray and proton beam scattering effects with TOPAS Monte Carlo simulation

For LBNL radiation biology research

ABSTRACT

In order to quantitatively understand X-ray and proton beam scattering effects in the cell-irradiation experiments performed at the BELLA Center and BSE of the Lawrence Berkeley National Laboratory (LBNL), a Monte Carlos simulation code was developed via TOPAS MC. For both X-ray and proton beam irradiation, experimental results and simulations are compared in two aspects, spatial dose distribution and absolute dose to the cell samples. The simulation reproduced the dose profile obtained in the experiments. The enhanced dose due to the scattering was also reproduced with the simulation. For X-ray scattering, the enhancement of the absolute dose was agreed within 14% for the "sandwich" case, and within 5% for the "behind" case. Considering the error on the experiments being >10%, this agreement is exceptionally good. For proton beams, scattering effects were found insignificant. The simulated dose profile agreed with the experiments quite well. Data collected from this scattering study allowed for a more precise understanding of the dose distribution and measurement and will provide a higher degree of control in future applications.

Zachary Kober
SULI Fall 2020
Research Paper

Zachary Kober
SULI Fall 2020
Research Paper Draft

I. INTRODUCTION

The study of laser-plasma driven ion acceleration (LPA) has shown potential for a great number of applications in both the physical sciences and medical field [1]. The reduced facility size and ultra-short duration of LPA beams in comparison to conventional ion accelerators makes them a good candidate for cancer therapy. Improvements in radiotherapy (RT) technology over the past few decades have resulted in an increased beam energy and target precision allowing for the safe delivery of higher doses to malignant cells. Recent studies suggest that an ultrahigh dose-rate irradiation RT called "FLASH" has been shown to decrease normal tissue damage while providing a standard tumor response expected from conventional dose rates [2, 3].

The study of FLASH RT has been pursued at Lawrence Berkeley National Laboratory's (LBNL) BELLA center through a collaboration with the Biological Systems and Engineering division. The research team has developed a platform where Flash RT can be studied based on LPA proton beams using the BELLA PW Ti:Sapphire laser system [4, 5]. The goal of this experiment is to understand the underlying mechanisms of the FLASH phenomenon through an exploration of the differential responses between normal cells and tumor tissues in vivo. Initial irradiation experiments were conducted, and LPA proton beams (Flash RT) were compared to a conventional X-ray machine (non-Flash RT) using in vitro cell samples with the same integrated dose. Data analysis from this first experiment is ongoing, and the initial analysis results have indicated that a more detailed study in the following sub-topic is highly desired.

Experimental results suggested that scattering effects of the irradiation beam on the target had a significant impact on the observed data, especially for the X-ray irradiation. A Monte

Carlos simulation code was developed via TOPAS MC [6] to better understand these scattering effects. This simulation code allowed for a comparative analysis between the experimental data and simulation results providing a quantitative and more accurate analysis of the dose.

This paper serves to explore the specifics and impact of the supplementary data gained through the Monte Carlo simulation on the larger set of empirical data gathered by the research team. Section II describes the materials and methods used to achieve these results. Section III presents the results and discussion, and Section IV discusses the potential for future applications pertaining to the setup and implementation of LPA systems capable of achieving the FLASH effect.

II. MATERIALS AND METHODS

A Monte Carlo simulation of the experimental irradiant setup for the X-ray and proton beams (Fig. 1) was developed through TOPAS MC version 3.5 and implemented on a Windows 10 system using Ubuntu 20.04 Linux environment. Simulation runs were completed on an Intel® Core™ i7-9750H CPU taking advantage of TOPAS's multithreading capability to use 11 of the 12 logical processors. Component materials were based on TOPAS default parameters unless specified in Table 1 [9]. Experiment specific geometries were built as CAD components using Autodesk Inventor Pro 2021 and implemented as high resolution STL files. Each simulation trial was completed on a different random number seeds to ensure robust data. A high history count was achieved through sequential runs. For both beam configurations, a modified default physics module was selected ("g4em-standard_opt4" "g4h-phy_QGSP_BIC_HP" "g4decay" "g4ion-

binarycascade" "g4h-elastic_HP" "g4stopping" "g4radioactivedecay") and the target was scored using the sum of energy deposits divided by the mass [10, 11].

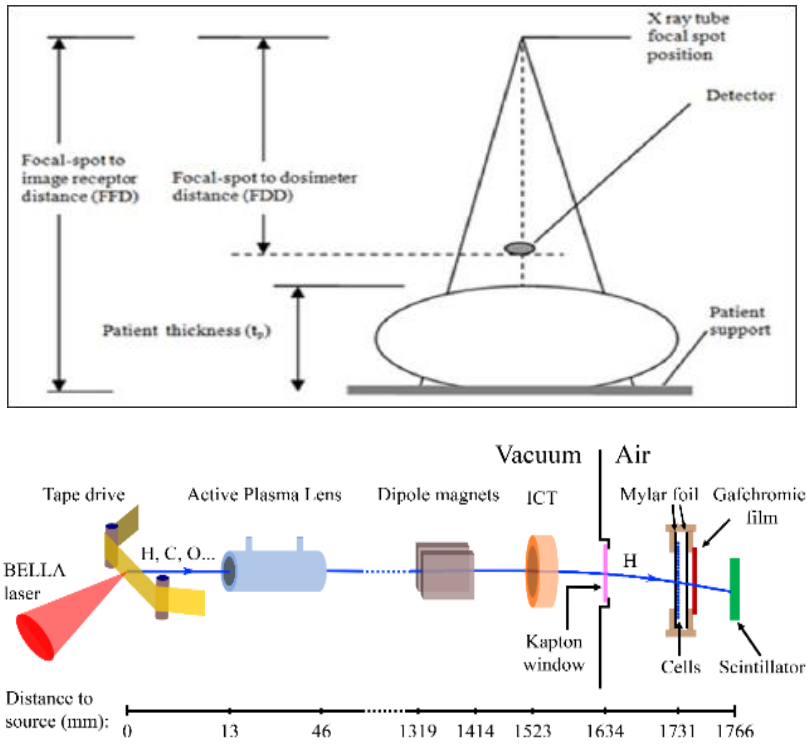

Figure 1: (a) Schematic of the X-Ray Irradiation beam setup created using an X-Rad 320 Biological Irradiator. The RCF was placed at the FDD Distance approx. 50 cm from the X-Ray focal spot. (b) Schematic of the high-repetition-rate laser driven proton beamline.

Table 1: Material Composition by Element Percentage Weight

Material	Cr	Ni	C	Mn	Si	P	S	O	N	H	Li	Na	Cl	Al	Ar	Density (g/cm^3)
Stainless Steel (304 Austenitic)	19	10	0.15	2	0.75	0.045	0.03		0.1							8.06
Buna N Nitrile (32% Acrylonitrile)			82.2						8.34	9.45						1.17
HDv2 GafChromic Film (Active)			27.6				0.1	11.7	0.4	58.2	0.6	0.5	0.6	0.3		0.8641
HDv2 Film Polyester Substrate			43.4					17.5		38.8	0.1	0.1	0.1			1.2595
Dry Air (ICRU-104)			1					25	70.54						3.46	0.001204

A. X-ray Setup

The X-ray setup for the Monte Carlo simulation is based on Figure 2. The RCF was scored in three different configurations to provide a benchmark, scattering reference and calibration of the HDv2 Film. The three-component target holder made of Aluminum, Austenitic 304 Stainless Steel and fitted with Buna N Nitrile 70 Duro Shore A (rubber) seals was designed and implemented as CAD components (Fig. 3). The HDv2 GafChromic film was built using TOPAS geometries and made to match the height and width of the target holder. The X-ray source was propagated through air with beam specifications shown in Table 2.

The simulation was conducted with the target perpendicular to the collimated X-ray beam source at a distance of 50 cm from the front plane of the first RCF (as in the sandwich and no holder configurations). The RCF was irradiated with a total history count (number of particles) of $2x10^8$ per trial. The total particle count and accurate dose distribution was further estimated by combining the random seed data from multiple sequential trials per configuration for a total combined particle count of 1.6 billion. The total dose sum for the X-ray Monte Carlo simulation was estimated such that each particle represented 10^5 particles in the real experiment and acquired data were adjusted accordingly. For each trial the RCF target was scored as both a cumulative dose sum and binned in two dimensions for a dose distribution per area (Sample was subdivided into 240 x 500 x 1 rectangular prisms for a total resolution of 120,000 Bins). Binning data was further analyzed in MATLAB R2020a to produce a dose distribution plot of the recorded dose energy per bin. Normalized data was compared with experimental reference scans to further evaluate the scattering effects caused by the target holder.

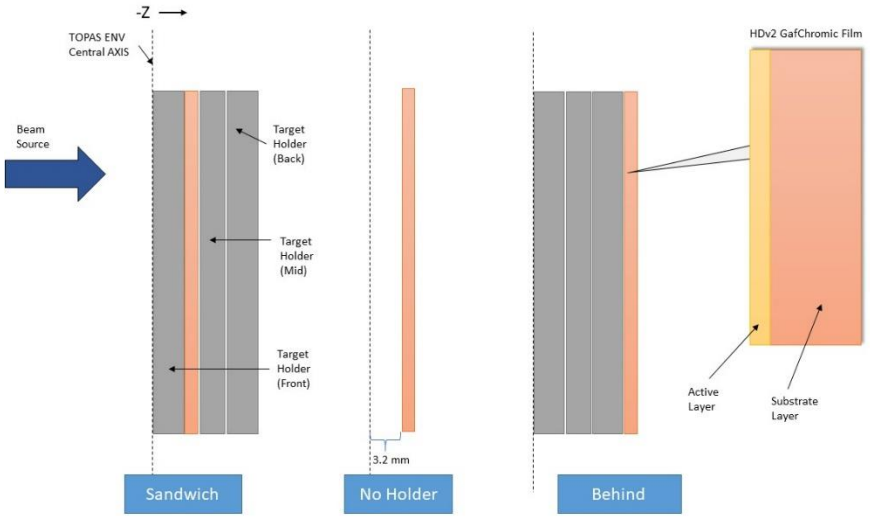

Figure 2: Schematic of x-ray beam setup for the Monte Carlo simulation. The sandwich configuration provides a reference for cell irradiation, the no holder configuration acts as a low dose RCF calibration with no scattering reference and the behind configuration is used as a benchmark.

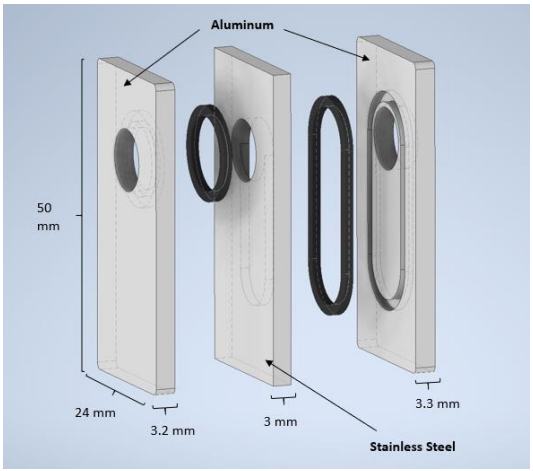

Figure 3: X-ray target holder CAD components used in Monte Carlo Simulation consisting of a front, middle and black plate as well as two rubber seals.

Table 2: X-ray beam source specification

Beam Particle Type	Gamma
Beam Energy	0.165 MeV
Beam Energy Spread	54.54545455
Beam Position Distribution	Flat
Beam Position Cut Off Shape	Ellipse
Beam Position Cut Off X (Beam Radius)	28 mm
Beam Position Cut Off Y (Beam Radius)	28 mm
Beam Angular Distribution	"None"
Beam Angular Cut Off X	0. Deg
Beam Angular Cut Off Y	0. Deg

B. Proton Beam Setup

The proton beam setup for the Monte Carlo simulation is based on Figure 4. The RCF was scored in three different configurations to provide scattering data and a calibration of the HDv2 Film. The behind configuration has an additional 5-micron water layer on the interior of the first mylar sheet matching the area or the target holder aperture to replicate the cell layer seen in experimentation. This configuration also contains slightly dryer air trapped in the air pockets of the closed target holder (Table 1). The three-component target holder used is identical to the one implemented in the X-ray simulation (Figure 3). The HDv2 GafChromic film sheets and 3.6-micron mylar layers were constructed with TOPAS geometries and made to match the height and width of the target holder. In order to emulate the energy spectrum, multiple incident particle angles and locations seen in experimentation a multi-beam implementation was used for the proton Monte Carlo setup. This beam setup (Figure 5) was passed through a 25 um Kapton Polyimide Film (ICRU-179) before being propagated through air with beam specifications shown in Table 3.

The simulation was conducted with the target perpendicular to the proton beam source at a distance of 97-mm from the end of the Kapton sheet to the front plane of the first mylar layer. The target was irradiated with a history count of $5x10^7$ per trial. The total number of particles per trial was distributed per beam to match the energy spectrum seen in experimentation (Table 3). The total dose sum for the proton Monte Carlo simulation was estimated such that each particle represented 10^2 particles in the real experiment and acquired data were adjusted accordingly. As in the X-ray simulation the RCF target was scored as both a cumulative dose sum and binned in two dimensions for a dose distribution per area at the same binning resolution. Binning data was further analyzed in MATLAB R2020a to produce a dose distribution plot of the recorded dose energy per bin. Data was compared with experimental reference scans to further evaluate the scattering effects caused by the target holder.

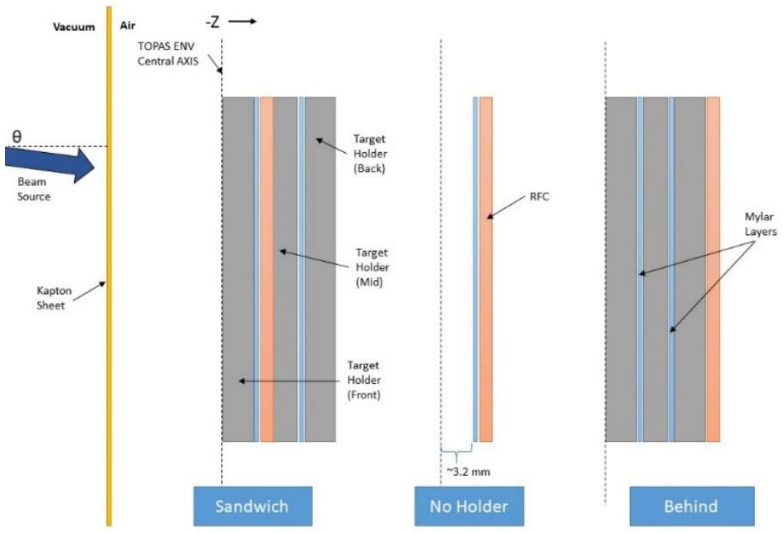

Figure 4: Schematic of proton beam setup for the Monte Carlo simulation. The sandwich configuration demonstrates the scattering effects in the middle of the target holder apparatus, the no holder configuration acts as a reference for no scattering and the behind configuration is used for the cell irradiation experiment. Not depicted in figure: the behind configuration has a 5-um water layer on the interior of the first mylar sheet and contains a dryer air than outside of the target holder.

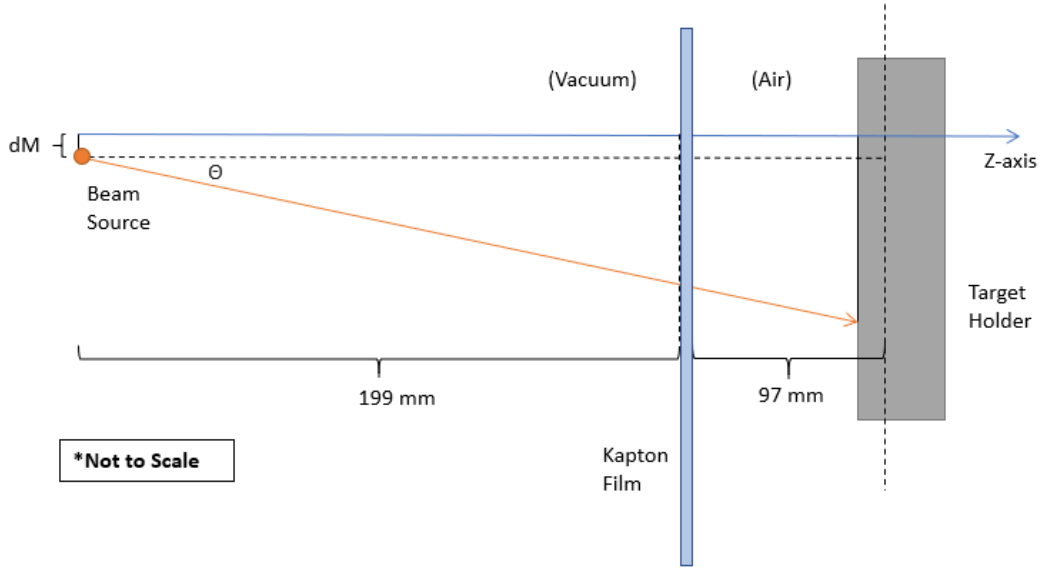

Figure 5: Multibeam setup for the Proton Monte Carlo simulation. Each beam source propagates through a vacuum before it passes through a Kapton window into air and is incident on the target holder aperture. Each beam has a different angle (θ), energy, and offset (dM) (due to the magnetic field (Figure 1b)), Table 3.

Table 3: Proton beam source specification

General Specification	
Beam Particle Type	Proton
Beam Energy Spread	0.0
Beam Position Distribution	Gaussian
Beam Position Cut Off Shape	Ellipse
Beam Position Cut Off X (Beam Radius)	12 mm
Beam Position Cut Off Y (Beam Radius)	12 mm
Beam Position Spread X (Standard Deviation)	6 mm
Beam Position Spread Y (Standard Deviation)	6 mm
Beam Angular Distribution	None

Beam Specific Specifications				
Beam Number	Angle, θ (deg)	Offset, dM (mm)	Energy (MeV)	Energy Spectrum
1	8.79421229	10.580752	2.7	39.4985 %
2	7.502355212	9.021621	3.7	27.6361 %
3	6.65071079	7.995062923	4.7	19.3362 %
4	6.03520272	7.253698	5.7	13.5290 %

III. RESULTS & DISCUSSION

A. Monte Carlo Simulation

Data gathered from the Monte Carlos simulation of the X-ray and proton beam setups was compared with experimental data from the research team. The dose profile and absolute dose, when compared to the no holder configuration, was used as a metric to determine scattering effects. Comparative analysis was done using a normalized dose distribution from each configuration (Sandwich, No Holder, and Behind RCF) of the Monte Carlo simulation for both setups. These normalized results were plotted in MATLAB against the (normalized) empirical data to examine differences along the exposed RCF of the target holder aperture. Simulation results from both setups were also plotted against one another to get a better understanding of the change in distribution at each configuration and to further draw comparisons between what was seen in simulation and what was seen in experimentation. In part the accuracy of the TOPAS Monte Carlo simulation was based on the number of interrupted histories in comparison to the total number of particles used per trial. This data, presented in more detail below, along with other sources of error (Appendix A), was not included as error bars for either simulation as it was seen to be well below 1/100 of a percent for all trials.

B. X-ray Setup

Three different configurations were tested in the Monte Carlo simulation of the X-ray beam. A high particle count and accurate dose distribution was estimated by combining multiple sequential trials. Simulation to simulation comparisons from all three X-ray configurations can

be seen in Figure 6. Experimental comparison results to the simulation data presented in the sandwich RCF configuration, no holder RCF configuration, and the behind RCF configuration can be seen in Figure 7. Specific simulation data for each trial is presented in Table 4 with trials that showed a binning error, to be discussed in section IV, marked with an asterisk. Table 5 shows an absolute dose comparison of the no holder configuration taken over the area of the 1-cm aperture.

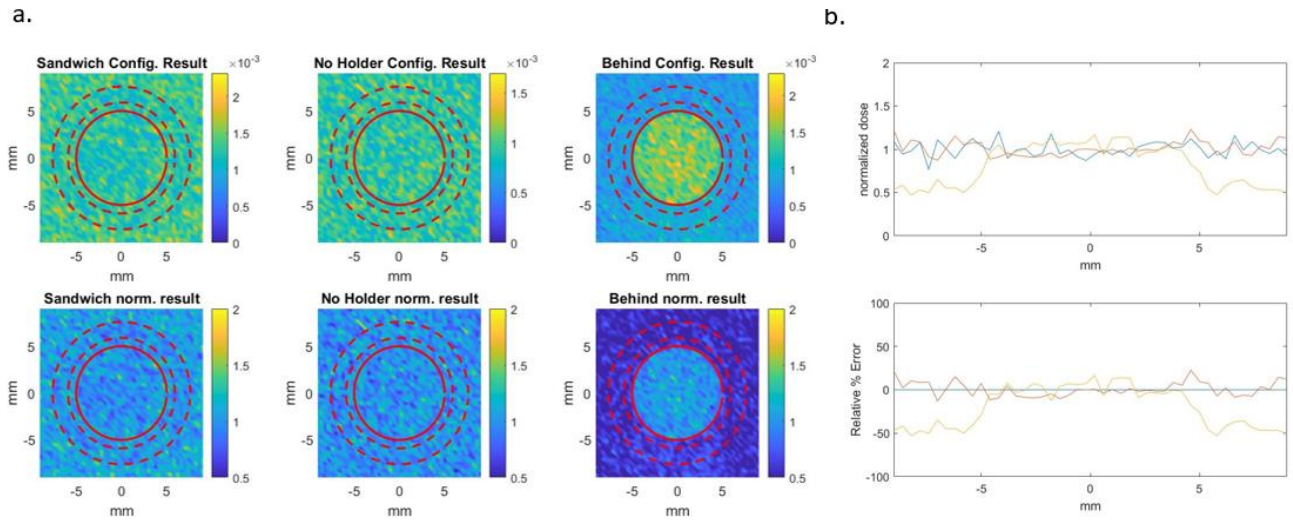

Figure 6: (a) Plotted dose distribution for each X-ray configuration simulation. The experimental and normalized distribution is shown in an 8x8 mm^2 section centered on the target holder aperture. (b) Normalized data from each simulation configuration is plotted together to allow for comparative analysis and to show the relative percentage change of dose along the RCF aperture using the no holder case as a reference. The orange plot is the sandwich config., yellow is the behind RCF config., and blue is the no holder reference. Simulation data resolution binning was decreased by 4x4 using MATLAB code to allow for a smoother distribution.

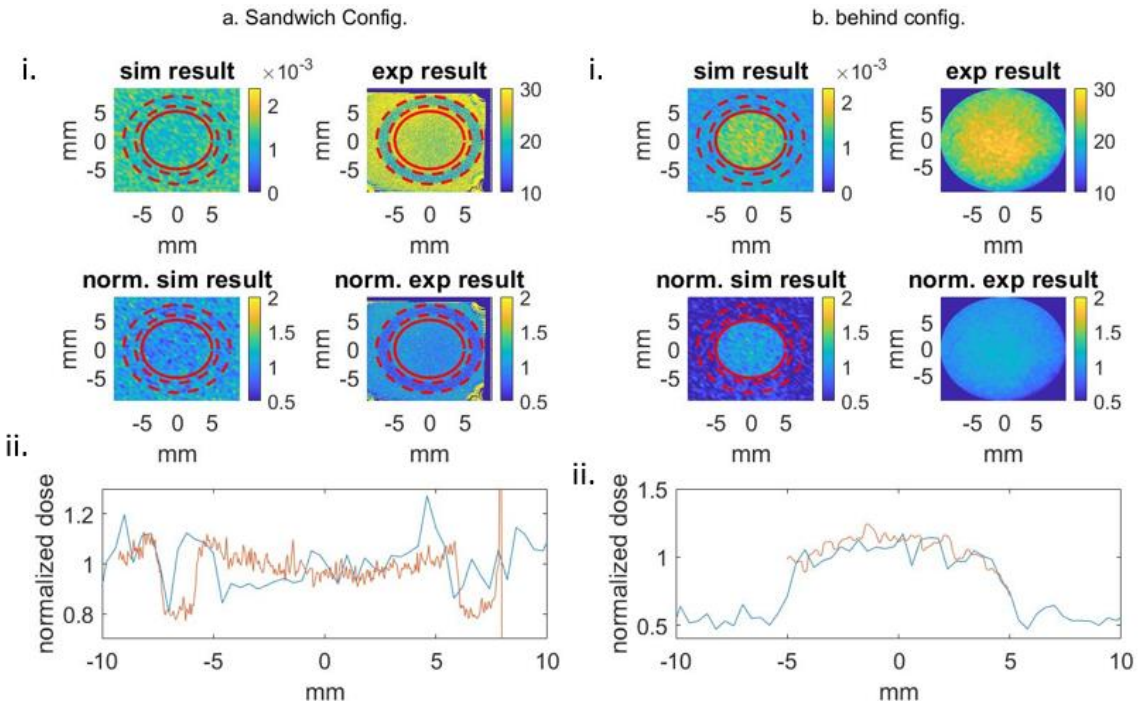

Figure 7: Simulation data resolution binning was decreased by 4x4 using MATLAB code to allow for a smoother distribution. (a)(i) Recorded and normalized dose distribution (in an 8x8 mm^2 section) for the X-ray sandwich configuration simulation compared with distribution data from the experiment. (ii) Normalized dose profile. Simulation data is in blue, experimental data is in orange (b) Dose distribution for the behind RCF configuration simulation compared with distribution data from the experiment.

Table 4: Trail Specific Data for the X-Ray Simulation of all Three Configuration

Sandwich RCF Configuration								
Seed	**1**	**2**	**3**	**4**	**5**	**6**	**7**	**8**
History Count	200M	200M	200M	200M	200M	200M	200M	200M
Inturrupted Histories	301	294	271	265	280	285	262	226
CPU Time (s)	41221.9	40025.6	41006.7	48830.2	49998.9	40152.1	49090.9	47657.1
Dose Sum (Gy)	8.55E-06	8.45E-06	8.60E-06	8.52E-06	8.62E-06	8.61E-06	8.55E-06	8.50E-06

Sandwich RFC	
Total History Count	1.6B
% Error	0.0001365
Net CPU Time (s)	357983.4
Net Dose Sum (Gy)	6.84E-05
Net Weighted Dose Sum (Gy)	6.84072

Behind RCF Configuration								
Seed	**1**	**2***	**3**	**4**	**5**	**6**	**7**	**8**
History Count	200M	200M	200M	200M	200M	200M	200M	200M
Inturrupted Histories	302	311	274	270	272	283	277	232
CPU Time (s)	48568.7	46659.1	46017.6	42852.3	45141.8	42290.7	46054.1	48074.6
Dose Sum (Gy)	5.67E-06	5.71E-06	5.69E-06	5.60E-06	5.70E-06	5.70E-06	5.74E-06	5.76E-06

Behind RFC	
Total History Count	1.6B
% Error	0.000138813
Net CPU Time (s)	365658.9
Net Dose Sum (Gy)	4.56E-05
Net Weighted Dose Sum (Gy)	4.55743

No Holder RCF Configuration								
Seed	**1***	**2**	**3***	**4***	**5***	**6***	**7***	**8**
History Count	200M	200M	200M	200M	200M	200M	200M	200M
Inturrupted Histories	0	0	0	0	0	0	0	0
CPU Time (s)	41585.4	47094.7	43119.1	47937.7	42083.6	46701.7	43313	48775.6
Dose Sum (Gy)	5.96E-06	6.03E-06	5.99E-06	6.00E-06	5.99E-06	6.06E-06	5.99E-06	5.98E-06

No Holder RFC	
Total History Count	1.6B
% Error	0
Net CPU Time (s)	360610.8
Net Dose Sum (Gy)	4.80E-05
Net Weighted Dose Sum (Gy)	4.79984

Table 5: Absolute Dose Comparison (average over 1-cm circle) for the X-Ray Simulation

Configuration	Aimed Dose (Gy)	Mean Dose (Gy)	Actual/Aim Ratio
X-Ray No Holder	-	6.0472	-
X-Ray Sandwich	6.0472	8.0167	1.326
X-Ray Behind	6.0472	9.4793	1.568

1. Discussion

Data presented in this section demonstrates a clear agreement between experimental and simulation data. The Sandwich RCF configuration exhibited an increase in absolute dose with a factor of 1.326 and presented the highest total dose seen by the RCF (Table 4, 5). Considering the ~10% error in experimental results this value was in good agreement with empirical data (Appendix B). Studies conducted during the setup of the Monte Carlo simulation showed scattering effects of the aluminum front plate dispersing particles at a range of up to 20-mm from the incident location. Secondary particles created from the low energy light-matter interaction of the X-ray beam and the target holder resulted in an overall increased dose when compared to the no holder benchmark [12].

Compare to experimental dose, Figure 7a, the simulation data was less robust than the experimental data, so the dose distribution was not a perfect match. However, the sandwich configuration did show consistencies along the aperture opening, with an overall decrease in dose and a slight buildup along the edges of the aperture creating a highly recessed “U” shape. Outside of the opening there were discrepancies in dose accumulation along the area of the rubber seal. Experimental results showed an approximate 10% decrease in dose from the baseline in this area where simulations results, Figure 6b, presented an approximate 10-15% increase in dose. As the rubber seal, when compared to the aluminum holder, has both a smaller density and

smaller atomic number the simulation results are more congruent with theory which indicates that this material should have a higher absorption rate and smaller scattering effect [13]. One potential explanation for this discrepancy is the type of RCF used in experimentation. The two-layer HD-v2 GafChromic film employed to capture the dose distribution relies on chemicals in the active later to change color upon irradiation. This active layer is not protected and has the potential to be "broken" or rendered ineffective by the pressure from the rubber seal [14]. This theory is currently being explored through further experimentation.

Simulation results for the behind configuration showed the lowest total dose but the highest absolute dose at the aperture opening with an increase over the no holder configuration by a factor of 1.568 (Table 4, 5). Consistent with these results, the experimental data (Appendix B) showed an average factor of 1.46 over all the target dose ranges and an average factor of 1.42 in the 8 Gy range. This is further supported by looking at the matching dose profile from the experimental data depicted in figure 7b (ii).

Using the simulation no holder configuration as a benchmark, Figure 6 shows a majority of dose centralized on the exposed RCF of the target opening with a clear increase along the center in an almost gaussian like distribution. This profile (Figure 7b) is in part due to the material composition of the target holder. Unlike the sandwich configuration, in the behind RCF case the X-ray particles must pass through both the front and back aluminum plate as well as the center stainless steel layer (Figure 3). This increase in material thickness and relative atomic number resulted in a decrease in the number particles passing through the holder and an overall decrease in total dose seen by the RCF. With the largest total volume of material for incident X-ray particles to interact with the scattering effects are most prevalent in this configuration.

C. Proton Beam Setup

As in the X-ray simulation three different configurations were tested for the proton beam. The dose distribution was created using a multibeam method to allow for several beam angles, locations, and energy levels. Simulation comparisons from all three proton configurations can be seen in Figure 8. Data comparisons between the simulation and experimental results for the no holder RCF configuration, and behind RCF configuration can be seen in Figure 9. In addition, simulation comparisons between the sandwich configuration and the dose experienced at the 5-um cell sample (behind configuration) can be seen in Figure 10. The sandwich RCF configuration was not tested by the research team and comparison between the cell layer and this configuration were done in simulation only. Specific simulation data for each trial for the proton beam setup is presented in Table 6 and an absolute dose comparison of no holder configuration taken over the 1-cm aperture area is seen in Table 7.

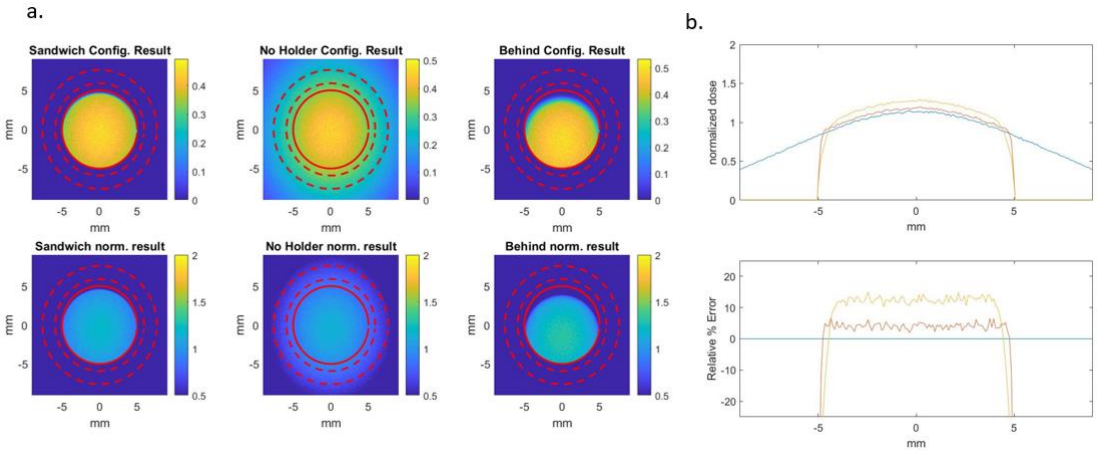

Figure 8: (a) Plotted dose distribution for each proton configuration simulation. The experimental and normalized distribution is shown in an 8x8 mm^2 section centered on the target holder aperture. (b) Normalized data from each simulation configuration is plotted together to allow for comparative analysis and to show the relative percentage change of dose along the RCF aperture using the No Holder case as a reference.

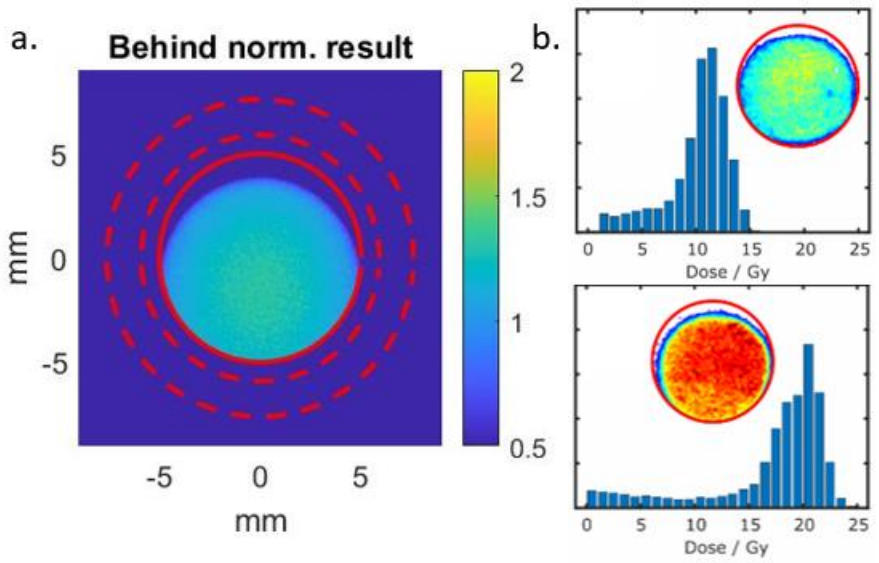

Figure 9: (a) The normalized distribution is shown in an 8x8 mm^2 section centered on the target holder aperture for the proton simulation "behind" configuration. (b) Behind configuration data from the experimental results.

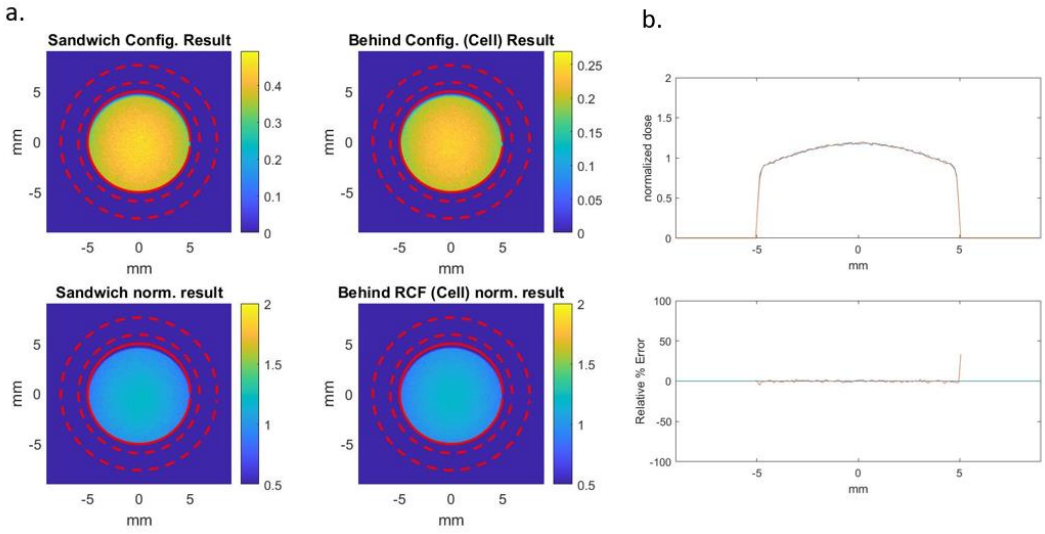

Figure 10: (a) The normalized data from the simulation is plotted together to allow for comparative analysis. (b) Dose profile plots for the sandwich configuration and the water cell layer. The sandwich is in blue, the cell is in orange.

Table 6: Trail Specific Data for the Proton Simulation of all Three Configuration

Configuration	History Count	Inturrupted Histories	CPU Time (s)	Dose Sum (Gy)	Weighted Dose (Gy)	% Error
No Holder	50M	0	35568.4	9.30E-02	9.30348	0
Sandwich	50M	1562	32753.2	2.48E-02	2.47503	0.0062
Behind RCF	50M	1338	30878	2.45E-02	2.44676	0.0054
Behind (Water Later)	50M	1407	39168.8	2.65E-02	2.64853	0.0056

Table 7: Absolute Dose Comparison (average over 1-cm circle) for the Proton Simulation

Configuration	Aimed Dose	Mean Dose	Actual/Aim Ratio
Proton No Holder	-	2.5693	-
Proton Sandwich	2.5693	2.4666	0.960
Proton Behind	2.5693	2.4356	0.948
Proton Behind (Water Cell)	2.4666	2.6394	1.070
No Holder (R= 4.5 mm)	-	2.1355	-
Sandwich Shadow OffSet, 0.2mm (R= 4.5 mm)	2.1355	2.1391	1.002
Behind Shadow OffSet 0.5mm (R= 4.5 mm)	2.1355	2.2576	1.057

1. Discussion

The proton setup for the Monte Carlo simulation required significantly more factors to be included to accurately emulate the experimental setup. As seen in Figure 1b particles are initially offset by a magnetic field before becoming incident on the 25-um Kapton polyimide film. Each particle leaves the film with a different energy and angle before propagating through air and interacting with the target. Higher energy particles are offset less by the magnetic field and end up hitting the target higher up where lower energy particles, more affected by the magnetic field, are deflected downwards. Data from Figure 8b showed the no holder case to be in good agreement with the empirical data, presenting a gaussian like distribution along the aperture with an overall elliptical shape from the predicted high and low energy levels hitting different points on the target.

Like the X-ray simulation, data presented in this section showed a clear agreement between experimental and simulation data. Referencing Figure 8, the sandwich configuration showed a margin increase in dose profile (approx. 3-4%) with a similar distribution to the no holder benchmark but an overall decrease in absolute dose by a factor of 0.96. This increase in profile but decrease in absolute dose is due to the shadow effect of the target holder. Protons are an ideal particle for ion irradiation as they have the highest charge to mass ratio and are therefore the easiest to accelerate [1]. Unlike the X-rays irradiation Protons have less penetrating power and, at the energy range relevant to this experiment, are completely stopped by the aluminum target holder. Unable to penetrate the target holder, the proton beam appeared to leave a small crescent shaped shadow at the top of the aperture opening reflecting the varied angles of the incoming particles. This shadow reduced the total number of particles hitting the opening and required a dose offset compensation to make a good comparison to the no holder benchmark.

The behind configuration displayed this same shadow but to even greater effect as the particles had to travel a larger distance to reach the back of the target holder apparatus. Compared to the no holder case the behind configuration showed the largest increase in dose profile (approx. 11-12%) and presented a similar decrease in absolute dose ratio by a factor of 0.948. Data presented in Figure 9 showed the simulation results to be in good agreement with the experimental scans. When looking at the absolute dose over a range that does not include the shadow, the sandwich and behind showed more expected results (Table 7). The behind configuration had the largest absolute dose, and the sandwich had the second largest compared the no holder benchmark. Having an understanding of the absolute dose at each location is

significant because it allows for the "dose on cell" (you can't measure) to be deduced from the "dose on RCF" (what we can measure).

Looking at the dose experienced by the 5-um water cell in the behind configuration, when compared to the sandwich RCF data (Figure 10) the dose distribution was incredibly similar with less than 1% change in dose profile across the aperture. However, the dose experienced by the cell (Table 6, 7) was higher than the sandwich RCF layer by a factor of 1.1. This increase in absolute dose has to do with its relative thickness and material properties of the water layer when compared to the RCF. This value can be used to better understand the dose on cell deduced from RCF experimentation.

V. CONCLUSION

Monte-Carlo simulations for ATAP-BSE radiation biology experiments were carried out to gain quantitative understanding on the x-ray and proton beam scatterings. These effects are studied by comparing the dose distribution and absolute dose on the targets. For X-ray scattering, the dose profile observed in experiments were reproduced by the simulation very well. The enhancement of the absolute dose was agreed within 14% for the “sandwich” case, and within 5% for the “behind” case. Considering the error on the experiments being >10%, this agreement is remarkable. For proton beams, scattering effects were found insignificant. The simulated dose profile agreed with the experiments quite well. This work has provided quantitative understanding on the scattering effects. In addition, it laid foundations of Monte-Carlo simulation work for future

experiments. Any minor modifications of the setup can be modeled readily, and the effects of scatterings can be simulated and understood quantitatively.

VI. APPENDIX

A. Sources of Error

The Monte Carlo simulation of the X-ray and proton beam setup was meant to provide an in-depth analysis of the scatting effects caused by the target holder apparatus and give a better understanding of the recorded dose. Before discussing more general potential sources of error present in this simulation it is worth noting the discrepancies in data collection between the X-ray and proton setup as seen in the Section III results. Data presented in this section showed that the X-ray simulation was not able to achieve the same smooth distribution that was seen in the proton simulation.

The XRAD-320 biological irradiator used for the X-ray experimentation allowed for large area irradiation. In order to emulate this setup and capture the scattering effects seen in experiments, a fairly large area was needed for the simulation (Table 2). As the total particle count available per trial (Table 4) was constrained by time and hardware limitations increasing the beam diameter effectively created a less dense particle distribution. Unlike the proton setup X-ray irradiation does not generate as many secondary particles and primarily relies on the photoelectric and Compton effect to turn electrons into secondary (beta) particles that can ionize other atoms [15] so increasing the beam diameter had noticeable effects.

Monte Carlos simulations in general are not meant to perfectly replicate reality and instead allow one to simulate a large enough percentage of the total particles or dose needed to reach a desired uncertainty, and then scale up to a final dose from there [16]. In the case of this simulation, it was not possible to achieve a high enough particle count to allow for a perfectly smooth distribution. For the X-ray setup each configuration was run with a total 1.6 billion particles at scaling factor of 1:100,000 (Table 4). While this allowed for comparable and usable data, as previously discussed, a more ideal data set would contain a substantially larger number of particles providing a smaller scaling factor and smoother distribution. The inability to achieve a perfectly smooth distribution directly affected the mean dose across the aperture for the X-ray trials as there were far more patches of un-irradiated target compared to the experimental data.

Potential sources of error for the Monte Carlo simulation of both setups come from a variety of qualitative and quantitative sources. As discussed above there is a certain level of uncertainty due to the smoothness of the distribution that comes from simulating only a portion of the real experiment.

Another metric for capturing the accuracy of each simulation was to look at the number of interrupted histories presented in each trial. This number is generated from a track error where particles incident on a vertex, border or plane incorrectly pass through the geometry and are recorded without necessarily experiencing the same physics as the rest of the simulation. This error is entirely due to the implementation of CAD components into the Monte Carlo simulation. In TOPAS CAD components are imported as STL files which rely on a variety of points connected in a triangular pattern to form planes which define a 3D surface [17]. Higher resolution STL files have more surfaces and are more likely to cause this error but do a better job

representing the shape of the component. Low resolution STL are less likely to cause this error but do a less accurate job replicating non flat surfaces or curves. While STL file format is compatible with TOPAS software TOPAS geometries are defined in a different manner that does not cause this issue. As seen in Table 4 and 6 this source of error, while present, was well below 1/100 of a percent for all trials.

Another source of error occurred from binning data being incorrectly recorded for a small percentage (maximum one bin) of the available 120,000 bins. Data for each trial was scored using two methods so incorrect binning data could be compared to a correct total dose sum to determine what the value of the missing bin should have been. As this simulation was focused on understanding the dose distribution along a certain area (8x8 mm^2 section centered on the target holder aperture) data points well outside this range that presented incorrect binning data were simply set to zero. In the instance where an outlying data point was included in the range of interest (as in the X-ray Behind RCF) this point was solved for using the method described below. Here S_T is the dose total sum (the sum of the energy deposits, E_T divided by the total mass, M). A_B is the dose average over all the bins of data, N is the total number of bins, X_n is the dose per bin, and X_u is the unidentified bin value.

$$S_T = \frac{E_T}{M} \quad \text{Eq. (1)}$$

$$A_B = \sum_{n=1}^{B} \frac{X_n}{N} \text{ where } X_n = \frac{E_n}{M_n} \text{ as } M_n = \frac{M}{N}, \; A_B = \sum_{n=1}^{B} \frac{E_n}{M} = \frac{E_T}{M} \therefore S_T = A_B \quad \text{Eq. (2)}$$

$$A_B = \sum_{n=1}^{N} \frac{X_n}{N} = \sum_{n=1}^{N} \frac{X_1 + X_2 \ldots . + X_n}{N} = \frac{\sum_{n=1}^{N-1} X_n + X_u}{N} \quad \therefore \quad A_B = S_T = \frac{\sum_{n=1}^{N-1} X_n + X_u}{N} \quad \text{Eq. (3)}$$

$$X_u = S_T \cdot N - \sum_{n=1}^{N-1} X_n \quad \text{Eq. (4)}$$

As seen in the above equations the relationship between the total dose sum and the average dose sum across all bins allows for outlying data points to be found.

A final source of potential error for this Monte Carlo simulation lies in overall setup and underlying physics that govern particle interaction. While the material properties, locations and overall design of the Monte Carlo simulation was made to match the experiment as closely as possible much of the information gathered to build this setup was taken from SRIM [18] (Stopping and Range of Ions in Matter) data or supplied by a manufacturer. These sources do not account for any irregularities that may have been present in the actual experimental setup. In addition, the simulation only applies the physics dictated by the module selection, Section II, and does not account for all physics phenomena that might exist. While the module selection was intentional and heavily supported [10, 11] there is a possibility that certain aspects of reality were not included in the simulation results.

B. Experimental Data (Absolute Dose)

Table 8: Experimental data for X-ray sandwich and behind trials

	Sandwich			behind		
Aimed dose [Gy]	Measured dose [Gy]	Error [%]	dose enhancement	Measured dose [Gy]	Error [%]	dose enhancement
5	4.75	22.9	0.95	7.33	17.1	1.47
8	9.53	12.7	1.19	11.38	18.6	1.42
10	12.08	14.5	1.21	17.11	6.2	1.71
15	19.53	7.9	1.30	19.69	22.1	1.31
average			1.16			1.48

VII. ACKNOWLEDGEMENTS

This work was supported in part by the U.S. Department of Energy, Office of Science, Office of Workforce Development for Teachers and Scientists (WDTS) under the Science Undergraduate Laboratory Internship (SULI) program as well as the Laboratory Directed Research and Development (LDRD) funding from Lawrence Berkeley National Laboratory provided by the Director, and the U.S. Department of Energy Office of Science Offices of High Energy Physics and Fusion Energy Sciences, under Contract No. DE-AC02-05CH11231. I would especially like to thank Kei Nakamura for his advice and help throughout my scientific undergraduate laboratory internship (SULI) appointment and Antoine Snijders for supporting this position through Laboratory Directed Research & Development (LDRD).

VIII. REFERENCES

[1] H. Daido et al., "Review of Laser-Driven Ion Sources and Their Applications." *Reports on Progress in Physics*, vol. 75, no. 5, 2012, p. 056401., doi: 10.1088/0034-4885/75/5/056401.

[2] S.E. Diffenderfer et al., "Design, Implementation, and in Vivo Validation of a Novel Proton FLASH Radiation Therapy System." *The International Journal of Radiation Oncology, Biology and Physics*, vol. 106, No. 2. Pp 440-448, 2020., doi: 10.1016/j.ijrobp.2019.10.049

[3] A. Mazal, et al., "FLASH and Minibeams in Radiation Therapy: the effect of microstructures on time and space and their potential application to protontherapy." *The British Journal of Radiology*, vol. 93, no. 1107, 2020, p. 20190807., doi: 10.1259/bjr.20190807.

[4] K. Nakamura et al., “Diagnostics, Control and Performance Parameters for the BELLA High Repetition Rate Petawatt Class Laser”, IEEE J. Quantum Electronics 53, 1 (2017), doi: 10.1109/JQE.2017.2708601.

[5] S. Steinke et al., “Acceleration of High Charge Ion Beams with Achromatic Divergence by Petawatt Laser Pulses.” *Physical Review Accelerators and Beams*, vol. 23, no. 2, 2020, doi: 10.1103/physrevaccelbeams.23.021302.

[6] *TOPAS MC*, www.topasmc.org/.

[7] J.H. Bin et al., “Absolute Calibration of GafChromic Film for Very High Flux Laser Driven Ion Beams.” *Review of Scientific Instruments*, vol. 90, no. 5, 2019, p. 053301., doi: 10.1063/1.5086822.

[8] Cheung, Tsang, et al. “Post-Irradiation Colouration of Gafchromic EBT Radiochromic Film.” *Physics in Medicine and Biology*, vol. 50, no. 20, 2005, doi:10.1088/0031-9155/50/20/n04.

[9] “Default Parameters: Materials.” *Default Parameters - TOPAS 3.1 Documentation*, topas.readthedocs.io/en/latest/parameters/defaults.html?highlight=materials.

[10] Arce, P., et al. “Report on G4-Med, a Geant4 Benchmarking System for Medical Physics Applications Developed by the Geant4 Medical Simulation Benchmarking Group.” *Medical Physics*, 2020, doi:10.1002/mp.14226.

[11] Lansonneur, P., et al. “First Proton Minibeam Radiation Therapy Treatment Plan Evaluation.” *Scientific Reports*, vol. 10, no. 1, 2020, doi:10.1038/s41598-020-63975-9.

[12] “Template: Light–Matter Interaction.” *Wikipedia*, Wikimedia Foundation, 20 June 2020, en.wikipedia.org/wiki/Template%3ALight%E2%80%93matter_interaction.

[13] “Interaction of Radiation and Matter.” *Interaction of Radiation and Matter*, www.nde-ed.org/EducationResources/HighSchool/Radiography/interactionradmat.htm.

[14] Niroomand-Rad, et al. “Radiochromic film dosimetry: Recommendations of AAPM Radiation Therapy Committee Task Group 55” *Medical Physics*, vol. 25, no. 11, Nov. 1998, doi:0094-2405/98/25(11)/2093/23

[15] Mott, Vallerie. “Introduction to Chemistry: Modes of Radioactive Decay.” Lumen, courses.lumenlearning.com/introchem/chapter/modes-of-radioactive-decay/.

[16] Brownlee, Jason. “A Gentle Introduction to Monte Carlo Sampling for Probability.” *Machine Learning Mastery*, 24 Sept. 2019, machinelearningmastery.com/monte-carlo-sampling-for-probability/.

[17] “What Is an STL File?” *Sculpteo*, www.sculpteo.com/en/3d-learning-hub/create-3d-file/what-is-an-stl-file/.

[18] “Interactions of Ions with Matter.” *James Ziegler - SRIM &* TRIM, www.srim.org/.